

Wake Sensing for Aircraft Formation Flight

Maziar S. Hemati,^{*} Jeff D. Eldredge,[†] and Jason L. Speyer[‡]

*Mechanical & Aerospace Engineering, University of California, Los Angeles
 Los Angeles, CA, 90095-1597, USA*

It is well established that flying aircraft in formation can lead to improved aerodynamic efficiency. However, successfully doing so is predicated on having knowledge of the lead aircraft's wake position. Here, we develop a wake sensing strategy to estimate the wake position and strength in a two-aircraft formation. The wake estimator synthesizes wing-distributed pressure measurements, taken on the trailing aircraft, by making use of an augmented lifting line model in conjunction with both Kalman-type and particle filters. The various estimation algorithms are tested in a vortex-lattice simulation environment, thus enabling the effects of modeling error to be analyzed. It is found that biases in the position estimates no longer arise if a particle filter is used in place of the Kalman-type filters. Filter divergence is observed when the relative aircraft separations are held fixed. This divergent behavior can be alleviated with the introduction of relative aircraft motions, for example in the form of a cross-track dither signal.

Nomenclature

α	Angle of attack
$\alpha_{l=0}$	Two-dimensional zero-lift angle of attack
σ_v	Measurement noise standard deviation
σ_w	Process noise standard deviation
ΔC_p	Spanwise differential pressure coefficient
Γ	Lifting surface strength
Γ_o	Wake vortex strength
Ω_x	Roll rate
Ω_y	Pitch rate
b	Wake vortex separation distance
\tilde{b}	Wingspan
c	Chord length
\mathbf{k}_{cal}	Calibration Vector
m_o	Two-dimensional lift-curve slope
\mathbf{v}_k	Measurement noise vector, $\mathcal{N}(0, V_k)$
w_o	Wake-induced upwash
\mathbf{w}_k	Process noise vector, $\mathcal{N}(0, W_k)$
\mathbf{x}	State vector
y_o	Wake lateral coordinate
\mathbf{z}	Measurement vector
z_o	Wake vertical coordinate
H	Measurement Jacobian matrix
K_L	Airfoil constant, $\frac{1}{2}cm_o$
M_k	Estimation covariance matrix
V_y	Lateral velocity component

^{*}Graduate Student, Member AIAA.

[†]Associate Professor, Senior Member AIAA.

[‡]Professor, Fellow AIAA.

I. Introduction

Flying aircraft in formation can lead to significant fuel savings due to the reduction in induced drag realized by the trailing aircraft. This method of drag reduction is contingent upon having the trailing aircraft positioned properly within the upwash-field of the lead aircraft’s wake. The reduction in induced drag arising from flying aircraft in formation is, to first order, attributed to the rotation of the resultant force vector arising from the presence of the upwash-field associated with the lead aircraft’s wake.^{1,7} As depicted in Figure 1, the induced angle of attack due to the lead aircraft’s upwash-field leads to a decrease in induced drag (i.e. ΔD points in the direction of motion) and a small increase in lift. Many numerical and experimental studies have verified this reduction in drag.^{1,2,7,10}

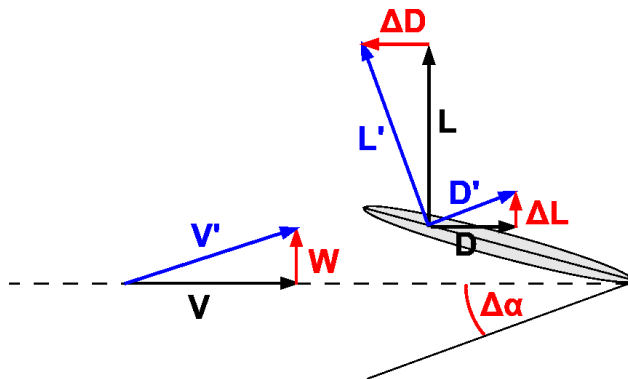


Figure 1: The upwash from the lead aircraft’s wake leads to a rotation of the resultant force on the trailing aircraft. To first order, this rotation is responsible for the decrease in induced drag realized by flying in formation.^{1,7} Baseline forces are drawn in black, induced effects are drawn in red, and formation forces are drawn in blue.

In considering autonomous formation flight, most studies have relied upon relative aircraft position measurements and previously acquired aerodynamic benefit maps, based on relative aircraft position. These approaches can operate reasonably well under ideal circumstances without subjugation to atmospheric disturbances and aircraft maneuvers, but they are not robust under more realistic circumstances. Surely, constructing the aerodynamic benefit maps is more useful if they are referenced relative to the wake position. The reason approaches have not relied on this framework lies in the fact that, to date, no reliable methods for wake estimation and sensing exist.

The technical objective of wake sensing is to obtain reliable estimates of the wake location based on measurements taken from a suite of on-board sensors. The ultimate goal is to rely solely upon pre-existing instrumentation; however, such a solution may not be physically possible. In the current development, wing-distributed pressure sensors are used to extract the lead aircraft’s wake parameters. Since the wake’s upwash-field is inherently distributed, the lead aircraft’s wake leaves an aerodynamic signature across the trailing aircraft’s lifting surfaces. By assimilating measurements from wing-distributed sensors, the wake signature can be used to back-out the wake location and other parameters of interest. The added advantage of such an approach is its ability to provide basic insights into the role of the fundamental wake nonlinearity associated with the upwash-field in the context of wake estimation. The wake estimation algorithm developed here makes use of simple, but rich, aerodynamic models to reveal the fundamental aspects of the wake sensing problem. We find that nonlinearities associated with the wake’s influence on the trailing aircraft lead to degraded filter performance, under certain circumstances. Adopting more sophisticated nonlinear filtering paradigms and introducing aircraft dynamics helps mitigate some of these issues. The present work marks the first time, to the authors’ knowledge, that distributed aerodynamic measurements have been synthesized to successfully determine the wake parameters of a lead aircraft during formation flight.

The design of the wake estimation algorithm is developed in Section II, beginning with aerodynamic modeling then followed by model integration with nonlinear estimation schemes. In Section III, we present

the resulting performance of several variations of the algorithm on formation flying aircraft configurations simulated by a vortex lattice method. Conclusions and future directions are discussed in Section IV.

II. Estimator Design

In designing a reliable wake estimation strategy, a representation of the wake's influence on the trailing aircraft must be considered. This representation will rely upon a model for the lead aircraft and its wake, as well as a model for the trailing aircraft's aerodynamic response due to the presence of this wake. The development of these models relies heavily on simple vortex entities such as line vortices and horseshoe vortices, which can be reviewed by the unfamiliar reader in Moran (1984) and Katz & Plotkin (2001). Upon constructing a sufficiently realistic representation of the wake-aircraft interaction, standard Kalman-type and particle filtering approaches from nonlinear filtering theory are invoked to define a suitable estimation algorithm.

In the current section, we begin by introducing a model for the lead aircraft and its wake in Section II.A. Next, in Section II.B, we introduce a lifting line representation for the trailing aircraft in the presence of the lead aircraft's wake. With a model for the aerodynamic response established, we integrate our model within the framework of various nonlinear estimation schemes in Section II.C. We consider Kalman-type filtering methods in addition to the particle filter. The various details of the wake estimation algorithms are discussed in the ensuing subsections.

II.A. Lead Aircraft and Wake Representation

The longitudinal separations experienced during formation flight missions are large enough to allow the wake to roll-up completely, thus making a horseshoe vortex model a reasonable representation of the lead aircraft and its wake. This can be further simplified by neglecting the influence of the bound vortex at large distances. In doing so, the semi-infinite horseshoe legs necessarily become infinite line vortices, with strength (Γ_o) and separation distance (b) dictated by the lead aircraft's weight and geometry, respectively. The expression for the upwash-field associated with this vortex wake can be obtained by linearly superposing the upwash-field associated with each infinite line vortex individually,

$$w_o(y; \Gamma_o, y_o, z_o, b) = \frac{\Gamma_o(y - y_o + \frac{b}{2})}{2\pi[z_o^2 + (y - y_o + \frac{b}{2})^2]} - \frac{\Gamma_o(y - y_o - \frac{b}{2})}{2\pi[z_o^2 + (y - y_o - \frac{b}{2})^2]}. \quad (1)$$

This nonlinear expression represents the wake's direct influence on the upwash-field as a function of the wake parameters Γ_o , y_o , z_o , and b (schematically defined in Figure 2). As will be seen, this nonlinear form is the fundamental nonlinearity associated with wake estimation.

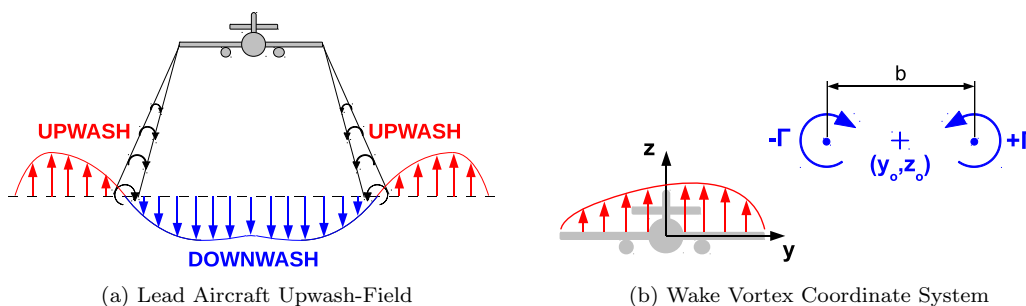


Figure 2: (a) The upwash-field attributed to the lead aircraft is equivalent to that of a horseshoe vortex. (b) The wake vortex system (blue) is defined with respect to the center of the trailing aircraft (gray). This wake leaves an aerodynamic signature on the lifting surfaces of the trailing aircraft (red) in the form of measurable quantities, such as distributions of differential pressure $\Delta C_p(y)$ or angle of attack $\alpha(y)$.

II.B. Trailing Aircraft Representation

With the lead aircraft's wake model established, it is now necessary to develop a mapping from the wake parameters to the trailing aircraft's aerodynamic response to the wake. This mapping is required for the estimation procedure and, ideally, will be of low computational cost. The physics of the problem lends itself to a classical lifting line approach, since we are only interested in studying slow time-scale (i.e. quasi-steady) maneuvers. The lifting line model also has the advantage of being able to capture distributed aerodynamic quantities through only a small number of Fourier modes, thus keeping the dimensionality of our model small enough for real-time implementation in the future. Here, we augment the classical model with Eq. (1) to accommodate the presence of a nearby wake.

Classical lifting line theory represents the vorticity of the wing and its associated wake by a spanwise distribution of horseshoe vortices. The lifting line integro-differential equations are then solved to determine the strength distribution along the lifting line. This strength distribution can then be used to compute other quantities of aerodynamic interest. The classical form of the lifting line equation is⁶

$$\Gamma(y) = \frac{1}{2}U_\infty c(y)m_o(y) \left[\alpha - \alpha_{l=0}(y) - \frac{1}{4\pi U_\infty} \oint_{-\tilde{b}/2}^{\tilde{b}/2} \frac{d\Gamma/d\eta}{y-\eta} d\eta \right], \quad (2)$$

with the boundary conditions,

$$\Gamma(-\tilde{b}/2) = \Gamma(\tilde{b}/2) = 0. \quad (3)$$

Eqs. (2) and (3) are only valid for a wing in free-space undergoing steady trimmed flight. If we wish to consider quasi-steady maneuvers in the presence of wake vortices, we must expand upon the expression above by introducing additional terms to the upwash distribution along the wing's span. For example, any vertical translational velocity V_z will introduce a uniformly distributed downwash along the span. Additionally, rolling maneuvers (i.e. rotations about the body-fixed x -axis) will induce a downwash proportional to the distance from the center of rotation $\Omega_x y$). Here we assume the center of rotation is located at the mid-span of the wing (i.e. $y_{C.G.} = 0$). Finally, pitching maneuvers (i.e. rotations about the body-fixed y -axis) will introduce a downwash proportional to the difference in position between the wing's center of gravity and the quarter-chord point $\Omega_y(c_{1/4}(y) - x_{C.G.})$. For our purposes, we will assume $c_{1/4} - x_{C.G.}$ is negligible, thus we will ignore this term. This assumption is also consistent with that of small sweep angles, which is inherent in the use of lifting-line theory in the first place. We finally include a term $w_o(y; \Gamma_o, y_o, z_o)$, which represents the upwash distribution associated with the presence of a finite set of line vortices to account for the presence of the wake.

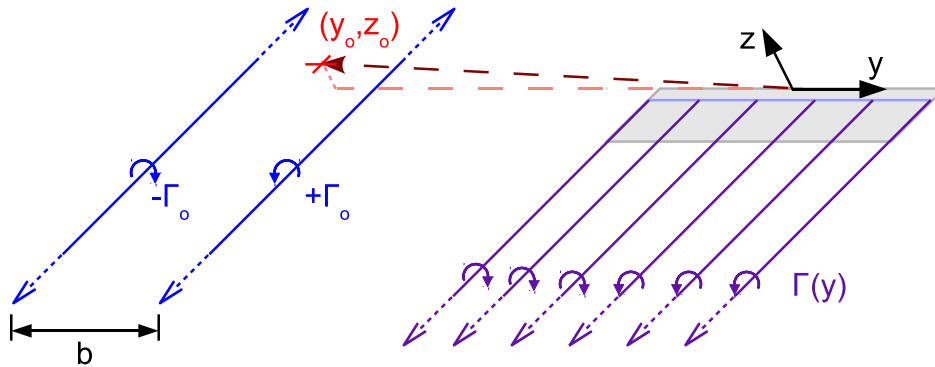


Figure 3: The augmented lifting line model is constructed via the standard lifting line vortex system (purple) with wake contributions resulting from a representative line vortex system (blue).

The final form of our generalized lifting-line integro-differential equation becomes,

$$\Gamma(y) = K_L(y) \left[U_\infty [\alpha(y) - \alpha_{l=0}(y)] - V_z - \Omega_x y + w_o(y; \Gamma_o, y_o, z_o) - \frac{1}{4\pi} \oint_{-\tilde{b}/2}^{\tilde{b}/2} \frac{d\Gamma/d\eta}{y-\eta} d\eta \right] \quad (4)$$

where $K_L(y) := \frac{1}{2}c(y)m_o(y)$, with the boundary conditions,

$$\Gamma(-\tilde{b}/2) = \Gamma(\tilde{b}/2) = 0. \quad (5)$$

The coefficient $K_L(y)$ can be replaced with a calibration coefficient, $K_{\text{cal}}(y)$, to allow for better predictions based on empirical data. Such a calibration allows the lifting line model to be used to predict $\Gamma(y)$ and associated aerodynamic quantities across the lifting surface of interest on an aircraft with multiple lifting surfaces. Further discussion of the calibration procedure is presented in Section II.C.5.

In the approach taken here, Equations (4) and (5) are solved by the collocation method.⁶ Once this integro-differential equation is solved for the $\Gamma(y)$ distribution, many other terms of interest easily follow. For example, it can be shown that for a flat plate the distribution of differential pressure coefficient will take the form

$$\Delta C_p(x, y) = -4 \frac{\Gamma(y)}{\pi U_\infty c(y)} \left(\frac{c(y)}{x} - 1 \right)^{1/2}. \quad (6)$$

II.C. Wake Estimation Algorithm

Having developed the necessary aerodynamic models, a viable estimation strategy based on various nonlinear estimation approaches can be developed. We first consider the class of Kalman-type algorithms due to their computational simplicity and ability to handle process and measurement uncertainty. A second class of estimators, utilizing particle filters, is also implemented to better handle the nonlinearities associated with the wake. All of the wake estimators developed in this work follow the same underlying approach (i.e. synthesizing distributed aerodynamic measurements with the aid of our augmented lifting line model), but do so by means of different nonlinear stochastic estimation algorithms.

Each of the following sections highlights an important aspect of the overall wake estimation strategy. We begin by defining the state and measurement vectors in Section II.C.1, followed by discussion of the associated measurement and process noise in Section II.C.2. Some necessary details related to Kalman-type and particle filters are presented in Sections II.C.3 and II.C.4, respectively. Further reading for the unfamiliar reader is cited in the respective sections of the two classes of algorithms. Regardless of the specific algorithm employed, we must perform an out-of-formation calibration prior to operating the wake estimator. Discussion of this process is presented in Section II.C.5. Finally, we discuss the specific aircraft dynamics considered in Section II.C.6.

II.C.1. States and Measurements

For the current discussion, we decide upon the following definitions,

$$\mathbf{x} := \begin{bmatrix} \Gamma_o \\ y_o \\ z_o \end{bmatrix} \in \mathbb{R}^3 \quad \text{and} \quad \mathbf{z} := \begin{bmatrix} \Delta C_{p_1} \\ \vdots \\ \Delta C_{p_i} \\ \vdots \\ \Delta C_{p_M} \end{bmatrix} \in \mathbb{R}^M. \quad (7)$$

Here, the states to be estimated are those associated with the relevant vortex parameters (see Figures 2 and 3)

1. The strength of the pair, Γ_o , and
2. The lateral and vertical positions of the wake origin (i.e. the center of the vortex pair) relative to the aircraft's body-fixed coordinate system, (y_o, z_o) .

Though we are mainly concerned with estimating the relative position of the wake, the associated vortex strength is an additional, but necessary, parameter to be estimated. Future investigations may consider other wake parameters, such as relative yaw angle and vortex spacing, as well.

In the current implementation, we choose to use the spanwise differential pressure distribution as the measurement. The reason for this choice lies in simplifying the estimator's development process. Since the $\Gamma(y)$ distribution solved for within the lifting line model is directly related to $\Delta C_p(y)$ via equation (6), we have chosen the differential pressure distribution as the measurement within the current framework. Other measurements, such as angle of attack distribution, may also have merit. More importantly, the current algorithms are not restricted to distributed measurements alone; however, the use of distributed

measurements allows valuable insights to be gained, so it is useful to consider such approaches first. If estimators relying upon distributed measurements lack in performance, then relying upon measurements of integrals over these distributions (i.e. lumped quantities, such as forces and moments) will be even more lacking. Although the ultimate hope is to rely exclusively upon existing on-board instrumentation for measurement data, validation under the distributed measurement framework must come first.

II.C.2. Measurement and Process Noise

We wish to design a wake estimator that is robust to both measurement and process noise. As such, we must model such effects within our estimator. The Kalman-type and particle filtering algorithms already take such effects into account. In our development, the process noise is currently only accounted for through the process covariance matrix, $W_k \in \mathbb{R}^{3 \times 3}$. No additive process noise is explicitly added within the system model. In an effort to keep the filter open, we always set $W_k > 0$. Since there is no process noise explicitly introduced within the simulation framework, W_k can be considered as a tuning parameter to be used in conditioning the filter for better performance.

Unlike the process noise, the measurement noise *is* explicitly introduced within the simulation. That is, the inputted measurement is assumed to have a white-noise signal, $\mathbf{v}_k \sim \mathcal{N}(0, V_k)$, added to it. Here, we assume the measurement has a “true” covariance of $V_k^{\text{true}} \in \mathbb{R}^{M \times M}$ when introducing noise to the measurement; however, within the filtering framework, we treat V_k as a tuning parameter. As such, V_k as defined within the context of the filter is not necessarily equal to V_k^{true} , and can be used to tune the filter.

We finally assume that our initial estimate for the vortex parameters is $\hat{\mathbf{x}}_o \sim \mathcal{N}(\bar{\mathbf{x}}_o, M_o)$. Again, the true estimate may have an initial covariance $M_o^{\text{true}} \in \mathbb{R}^{3 \times 3}$, but we choose to treat M_o only as a tuning parameter within the context of the filter. That is, we assume that any modeling error can be accounted for with a suitable choice of M_o in the filter initialization.

II.C.3. Kalman-Type Filtering: Measurement Function Linearization

Kalman-type filters are one class of nonlinear estimation algorithm in this study. In the interest of brevity, familiarity with Kalman-type filtering is assumed. The reader is referred to Jazwinski (2007) and Speyer & Chung (2008) for further details regarding such algorithms. In the present section, we only discuss computation of the measurement Jacobian matrix, H , which is required by Kalman-type filtering algorithms. For the vortex parameters \mathbf{x} given above, this takes the form,

$$H = \begin{bmatrix} \frac{\partial \Delta C_{p1}}{\partial \Gamma_o} & \frac{\partial \Delta C_{p1}}{\partial y_o} & \frac{\partial \Delta C_{p1}}{\partial z_o} \\ \vdots & \vdots & \vdots \\ \frac{\partial \Delta C_{pi}}{\partial \Gamma_o} & \frac{\partial \Delta C_{pi}}{\partial y_o} & \frac{\partial \Delta C_{pi}}{\partial z_o} \\ \vdots & \vdots & \vdots \\ \frac{\partial \Delta C_{pM}}{\partial \Gamma_o} & \frac{\partial \Delta C_{pM}}{\partial y_o} & \frac{\partial \Delta C_{pM}}{\partial z_o} \end{bmatrix} \in \mathbb{R}^{M \times 3}. \quad (8)$$

For the current implementation, we choose to compute the measurement Jacobian numerically. This is currently done via first order finite differences applied to small perturbations about the nominal (estimated) state.

II.C.4. Particle Filtering Procedure

The second class of nonlinear estimation algorithm considered in this study is the Particle filter (PF). Particle filters approximate the Bayesian optimal filtering equations by means of Monte Carlo methods. The *a posteriori* probability density is represented by a set of random samples, or “particles”, with associated weights. As the number of particles increases, the representation approaches the exact functional description of the probability distribution.⁸

As time progresses, the PF algorithm can lead to degeneracy due to overweighting a few samples, leaving the remaining ones useless. A common method of circumventing this issue comes in the form of a “resampling” step. The sequential importance resampling (SIR) PF algorithm implemented in the present study makes use of a simple cumulative sum algorithm to resample particles at every time step. Further details regarding particle filters and resampling algorithms can be found in Ristic et al.⁸

II.C.5. Offline Calibration

Thus far we have established all of the algorithmic details for the wake estimator. We are now left with the important step of ensuring that the model implemented within the estimator matches up with reality reasonably well. Thus, prior to “hooking up” the filter, the lifting line model within the filter needs to be *calibrated in an isolated flight configuration*. That is, the lifting line model must be calibrated against the actual measurement data offline in order to initialize the model for best performance. This is done by determining a linear gain vector ($\mathbf{k}_{\text{cal}} \in \mathbb{R}^M$) to apply to the model output,

$$\mathbf{k}_{\text{cal}} := \left[k_{\text{cal},1} \quad \dots \quad k_{\text{cal},i} \quad \dots \quad k_{\text{cal},M} \right]^T, \quad \text{where } k_{\text{cal},i} := \frac{z_{i,\text{Measured}}}{z_{i,\text{Lifting Line}}}. \quad (9)$$

Calibration is important in the case of both simulation and flight testing. Within the context of simulation, calibration allows the filter to better account for variations between aerodynamic models used to represent truth. Such calibration is also necessary for actual flight implementation because, in addition to modeling inaccuracies, unaccounted sensor biases may be present. In the case of pressure transducers, for example, such biases can be caused from installation or manufacturing errors. Calibrating the system offline introduces an element of robustness to the model because sensor biases can be better accounted for.

II.C.6. System Dynamics

We consider relative aircraft motions between two formation flying aircraft in some of our studies, which we describe in the present section. The system dynamics studied in the current effort are simply prescribed sinusoidal changes in the relative vertical and lateral displacements between the wing and wake axes. Moreover, the constant amplitude and frequency of the sinusoidal velocity by which the wing moves is assumed to be fully known (i.e. there is no variance associated with these parameters). The vertical velocity of the wing influences the induced drag and, therefore, the pressure measurements. This is accounted for within the lifting line implementation. The lateral velocity is prescribed only for the purpose of “increasing the observability” of the vortex pair. Such prescribed motions are expected to increase the observability of the vortex pair because, though $\mathbf{h}_k(\mathbf{x}_k)$ is not necessarily invertible for all values of \mathbf{x}_k , the prescribed motions are more likely to describe a set $[\mathbf{h}_1(\mathbf{x}_1), \dots, \mathbf{h}_{k-1}(\mathbf{x}_{k-1}), \mathbf{h}_k(\mathbf{x}_k)]$ that can only be generated from a unique set vortex parameters.

We denote the lateral and vertical velocity components of the wing as $V_y(t_k)$ and $V_z(t_k)$, respectively. For the purpose of simulation, we choose to move the wake with respect to the aircraft rather than to move the aircraft with respect to the wake. In doing so, we may ignore upwash/sidewash effects due to motions of the lifting surfaces. This provides a greater opportunity of distinguishing the wake’s upwash signature because it is less likely to be “washed out” by the presence of these additional disturbance-fields. Thus, for purposes of the estimator simulation, we can consider that the wing “sees” the vortex pair move with equal but opposite velocity components, ignoring all velocities due to motion of the solid bodies. Hence,

$$y_o^{(k+1)} = y_o^{(k)} - V_y(t_k)\Delta t_k \quad (10)$$

$$z_o^{(k+1)} = z_o^{(k)} - V_z(t_k)\Delta t_k. \quad (11)$$

In other words, the dynamical equations for this system can be written as,

$$\begin{bmatrix} \Gamma_o \\ y_o \\ z_o \end{bmatrix}_{k+1} = \begin{bmatrix} \Gamma_o \\ y_o \\ z_o \end{bmatrix}_k + \begin{bmatrix} 0 \\ -V_y(t_k)\Delta t_k \\ -V_z(t_k)\Delta t_k \end{bmatrix}. \quad (12)$$

Although other aspects of the aircraft dynamics have not been included here (e.g. roll and yaw kinematics), we plan to consider these aspects in future works. In the present study, only fundamental aspects of the filter have been considered. As such, we have dealt only with parameters that are expected to represent the capabilities of the filter, while keeping things as intuitive as possible.

III. Performance Results

Vortex lattice simulations of a generic aircraft equipped with five wing-distributed pressure sensors ($M = 5$) have been studied to assess the wake estimation algorithm’s performance characteristics. The simplest

possible aircraft is chosen for the present study because of the limitations associated with the classical lifting line approach in modeling sophisticated geometries such as sweep and dihedral. We note that the classical lifting line approach can be replaced with more sophisticated aerodynamic models (e.g. modern/extended lifting line methods or vortex panel methods) in the future. However, the classical lifting line method was selected due to its simplicity. Since the current focus is on the assessment of an estimation algorithm, the aerodynamic model must only be capable of capturing the class of nonlinearity associated with the process. Classical lifting line theory is entirely capable of doing this; it also provides a simple framework for tracking the influence of the fundamental wake nonlinearity on the overall estimator dynamics. By invoking this simpler model, we are also able to study the effects of modeling error on the estimator dynamics by testing the algorithm in a higher-fidelity simulation environment, such as the vortex panel method in the present work.

Two main types of simulations are considered in the vortex lattice results that follow:

1. Static configuration—there is no relative motion between the aircraft and wake.
2. Prescribed relative motions—relative kinematics are prescribed between the aircraft and wake a priori, thus introducing “dynamics”

In both of these instances, the same aircraft/sensor configuration is used (see Figure 4). The level of noise associated with the sensor measurements is also consistent in both cases. Process noise is not present in the simulation, though a finite “truth” process noise is assumed for use in tuning the estimator. The corresponding noise levels are

$$\sigma_v^{\text{truth}} = 1 \times 10^{-5}, \quad \sigma_w^{\text{truth}} = 1 \times 10^{-3}.$$

Unless otherwise stated, the estimator tuning parameters have the following values

$$\sigma_v = 7 \times 10^{-3}, \quad \sigma_w = 3 \times 10^{-2}.$$

Finally, all values are presented in dimensionless form, using wing span, flight speed, and air density at 28,000 ft as factors for non-dimensionalization.

III.A. Two-Aircraft Static Configuration

Several simulation results for the static configuration (i.e. no relative motions) are presented below. Case 1, presented in Figure 5 provides a validation for a simple configuration using an extended Kalman filter (EKF); the wake is close to the trailing aircraft, thus leaving a relatively strong signature on it. Based on both the estimation trajectory map and the error histories, we see that the estimator does a reasonable job zeroing in on the relative wake location. The estimate of the wake strength, however, does not perform as well. An interesting point to note is that this tends to be a common trend among most of the simulations conducted. Several studies were previously conducted, albeit briefly, on the effect of removing the wake strength Γ_o as a parameter to be estimated (i.e. assuming Γ_o is fully known). The results of these simulations, surprisingly, led to degraded estimator performance! As such, we will not consider such cases here. There are many questions that this introduces, though such quandaries will be saved for future investigations.

Case 2 considers a configuration with one and one-half wing spans of lateral separation and one wing span of vertical separation. Two different classes of nonlinear estimation algorithms were considered in this study: (1) Kalman-type filters and (2) particle filters. The Kalman-type filters consisted of an EKF, an iterated Kalman filter (IEKF), and a second-order Kalman filter (SOEKF). These three Kalman-type filters yielded similar results (only EKF results are presented in the interest of brevity), all of which led to significant biases or filter divergence depending on the initial estimates. The particle filter alleviated the bias issues, but divergence was still a problem. This indicates a potential unobservability that is not being handled properly by the sensor configuration, prompting need for further investigation.

III.A.1. Extended Kalman Filter

The EKF acting on Case 2, presented in Figures 6 and 7, reveals the presence of attractors in the estimation error space. The position estimate follows a similar trajectory for several different initial estimates and always leads to the same biased position estimate. In one of the cases presented, the estimate actually diverges! The wake nonlinearity and its associated observability structure are responsible for this behavior, though further investigation is necessary to determine methods for circumventing this structure.

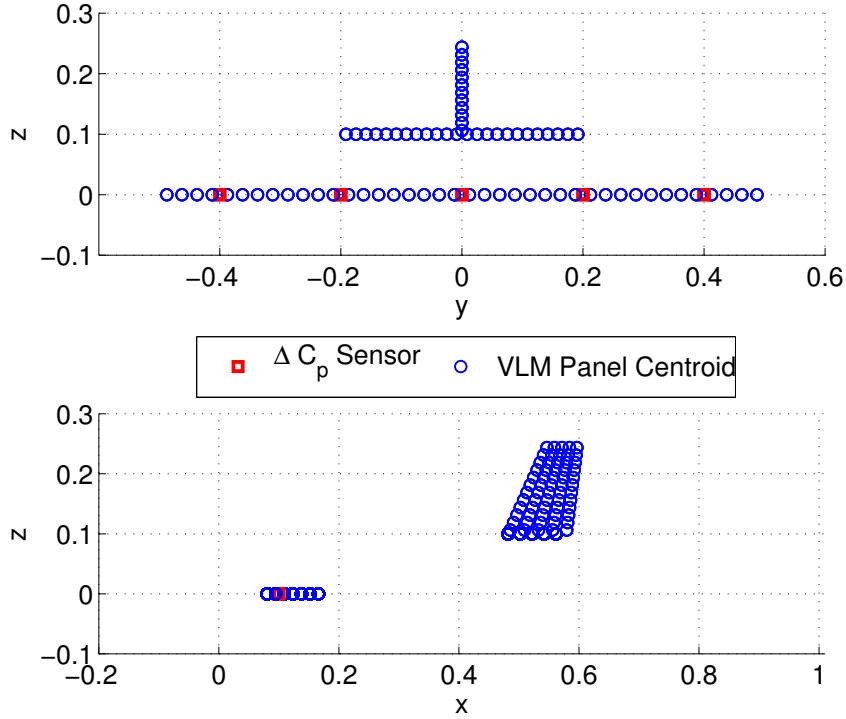


Figure 4: Aircraft configuration for the vortex panel simulation using five uniformly spaced wing-distributed pressure sensors. Vortex panel collocation points are denoted by \circ , while the five uniformly spaced pressure sensors are denoted by \square . The lower figure depicts the taper and sweep present in the vertical stabilizer as well as the relative position of the tail to the main lifting surface. All other lifting surfaces are untapered and unswept for the present study

III.A.2. Particle Filter

In implementing the PF for wake estimation, we set the following parameter values

$$N_p = 1000, \quad \sigma_v = 3 \times 10^{-4}, \quad \sigma_w = 1 \times 10^{-2}.$$

The PF results, presented in Figures 8 and 9, demonstrate the greatest performance among the four wake estimation algorithms studied. Because the PF propagates statistics through the vortex nonlinearity directly, without relying upon successive linearizations, the biases due to small modeling errors are minimized. However, as a result of system unobservability, the estimates continue to diverge along the magenta path. Future work must focus on reconciling this unobservability issue.

III.B. Two-Aircraft with Relative Motions

The following section considers the effect of relative motion on the performance of the wake estimation algorithm. It has been hypothesized that introducing relative motions between the aircraft and the wake leads to improvements in the wake's observability structure. As the aircraft moves closer to the wake, the signature should become more pronounced. Thus, a time sequence of wake signatures should be more revealing than a single wake signature with additive noise.

The prescribed relative motions are introduced as

$$\mathbf{x}_{k+1} = F_k \mathbf{x}_k + \Lambda_k \mathbf{u}_k$$

where

$$\begin{aligned}
 F_k &= I^{N \times N} \\
 \Lambda_k &= \begin{bmatrix} 0 & 0 \\ A_1 \omega_1 \Delta t & 0 \\ 0 & A_2 \omega_2 \Delta t \end{bmatrix} \\
 \mathbf{u}_k &= \begin{bmatrix} \cos(\omega_1 t) \\ \cos(\omega_2 t + \phi) \end{bmatrix}.
 \end{aligned}$$

In the interest of brevity, only the EKF results are presented here. Various values of A_1 , A_2 , ω_1 , and ω_2 are tested. The phase difference between the two channels is always chosen to be $\pi/4$ in the simulations presented here. A simple example of the incorporation of kinematics is presented via Case 3 (equivalent to Case 1, but with dynamics) in Figure 10. Although the estimate appears to lock in on the z_o value in terms of phase, the actual estimate has a periodic error value in steady-state. Though not apparent under such weak forcing magnitude, the unforced channels (i.e. Γ_o and y_o) also have periodic values appearing in steady-state.

We find that the divergent behavior of the estimator, seen in Figure 7, can be eliminated under certain kinematics (see Figure 11). However, the resulting converged estimate is far from the correct value. Figure 12 is presented to demonstrate the fact that kinematics does not guarantee convergence, as the simulation leads to estimator divergence under the prescribed kinematics defined here.

The mitigation of divergence through relative motions between wake and aircraft motivates further study in this area. Dynamics has an influence on the observability structure of the wake, as previously explained. As demonstrated in the results presented here, arbitrary motions are not enough to lead to performance gains. The influence of dynamics on system observability and estimator performance must be carefully studied if vortex-based wake estimation is to be successful in practice.

IV. Conclusions

The current study has made much progress in understanding the nature of wake estimation and in developing a viable wake sensing strategy based on distributed aerodynamic measurements. Multiple attractors have been identified in the estimation error space associated with Kalman-type filters acting on the wake nonlinearity. Particle filters have been shown to alleviate this resulting bias, though divergence issues associated with the wake observability structure still remain an issue. Relative motions between the aircraft and the wake can help reduce the issues with divergence, but do not alleviate estimation biases. Further study of the effect of relative motions on the observability structure of the wake and on the performance of the wake estimators is a necessary endeavor.

If future work leads to better wake observability via relative motions, it may be possible to use integrated values of the aerodynamic quantities to say something about the wake parameters reliably as well. For example, by integrating the pressure distribution, the forces and moments can be deduced. Since this is a linear operation of the pressures, it remains a linear mapping of the wake nonlinearity. Hence, such an approach will not change the underlying structure of the estimation problem in this respect. However, by relying upon forces and moments, much of the signature associated with the wake is lost, and greater complexity is introduced to the problem by reducing the fidelity of the measurements to be incorporated. The ultimate wake estimation algorithm will likely make use of both force and moment measurements as well as distributed aerodynamic quantities in order to make reliable estimates of the wake location.

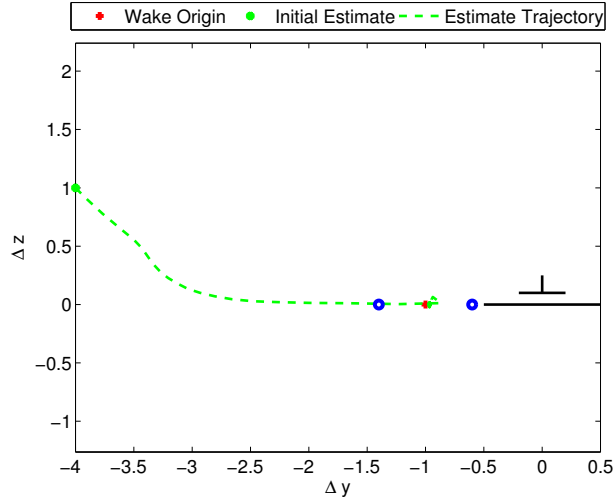
Though the effects of modeling error were studied by simulating the estimation strategy by means of a vortex lattice method, some classes of modeling errors were ignored. Prior to implementing the present estimation framework in physical experiments, it may be useful to consider the effects of wind gusts and transients, as well as wake-shape deformations, on estimator performance. The panel-particle method's ability to simulate the unsteady aerodynamics of multiple bodies and wakes will prove invaluable in conducting such studies.³

Additional improvements to the current wake estimators will come in the form of more sophisticated aerodynamic models. The present study only considers classical lifting line theory in the interest of simplicity. It was deemed necessary to develop an understanding of the wake's influence on estimator performance at a fundamental level, so it was decided to keep only as much sophistication as necessary to capture the essence

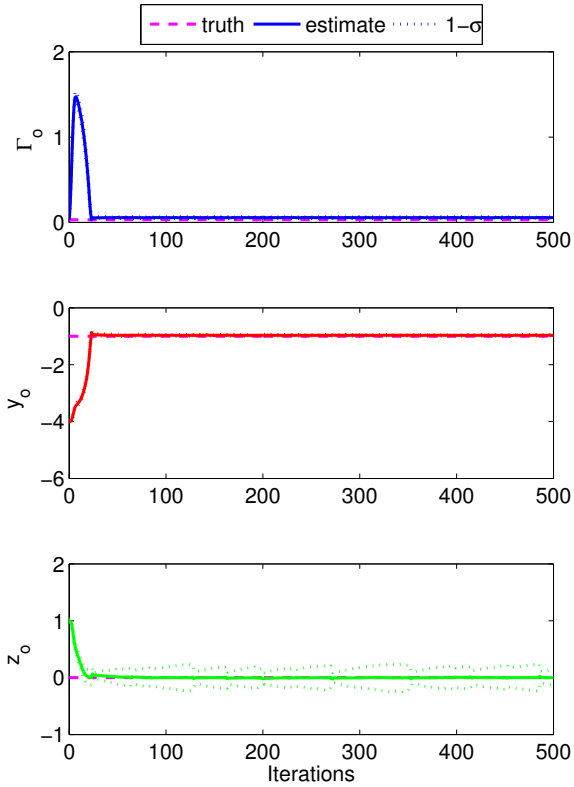
of the wake nonlinearity without additional complexity. In the future, extensions to modern/extended lifting line theory or to vortex panel methods will allow for added geometric complexity in the modeling of the aerodynamics for general aircraft configurations. Both of these methods are analogous to classical lifting line methods and operate on the wake nonlinearity in a similar manner to attain aerodynamic quantities of interest. Though the computational demand of these methods is greater than that of the classical lifting line method, several strategies exist for keeping the cost at a level amenable to real-time implementation. For example, the collocation matrices associated with panel methods can be precomputed, assuming the aircraft geometry itself does not undergo significant changes. Additional approaches may rely upon table look-ups for distributed aerodynamic quantities based on the set of vortex parameters; although, such methods tend to suffer from large memory burdens associated with storing the aerodynamic tables.

References

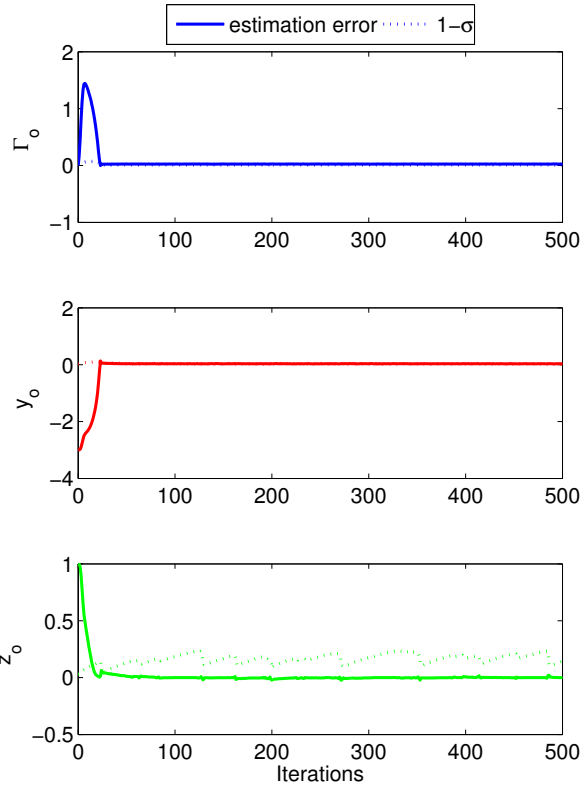
- ¹Blake, W. and Multhopp, D., “Design, performance and modeling considerations for close formation flight”, AIAA-98-4343, August 1998.
- ²Chichka, D.F., Wolfe, J.D., and Speyer, J.L., “Aerodynamically coupled formation flight of aircraft”, In *Proceedings of the 10th Mediterranean Conference on Control and Automation–MED2002*, Lisbon, Portugal, July 9–12, 2002.
- ³Hemati, M.S. and Eldredge, J.D., “A panel-particle method for studies of maneuvering aircraft formations”, In *63rd Annual Meeting of the Division of Fluid Dynamics*, volume 65, Long Beach, CA, November 21–23, 2010.
- ⁴Jazwinski, A.H., *Stochastic Processes and Filtering Theory*, Dover Publications, Mineola, New York, 2007.
- ⁵Katz, J. and Plotkin, A., *Low-Speed Aerodynamics*, ed. 2, Cambridge University Press, New York, 2001.
- ⁶Moran, J., *Introduction to Theoretical and Computational Aerodynamics*, John Wiley & Sons, New York, 1984.
- ⁷Ray, R.J., Bobleigh, B.R., Vachon, M.J., and St. John, C., “Flight test techniques used to evaluate performance benefits during formation flight”, Technical Report NASA/TP-2002-210730, NASA Dryden Flight Research center, Edwards, CA, August 2002.
- ⁸Ristic, B., Arulampalam, S., and Gordon, N., *Beyond the Kalman Filter: Particle Filters for Tracking Applications*, Artech House, Boston, 2004.
- ⁹Speyer, J.L. Chung, W.H., *Stochastic Processes, Estimation, and Control*, SIAM, Philadelphia, 2008.
- ¹⁰Vachon, M.J., Ray, R.J., Walsh, K.R., and Ennix, K., “F/A-18 aircraft performance benefits measured during autonomous formation flight project”, AIAA-2002-4491, August 2002.



(a) Estimate Trajectory

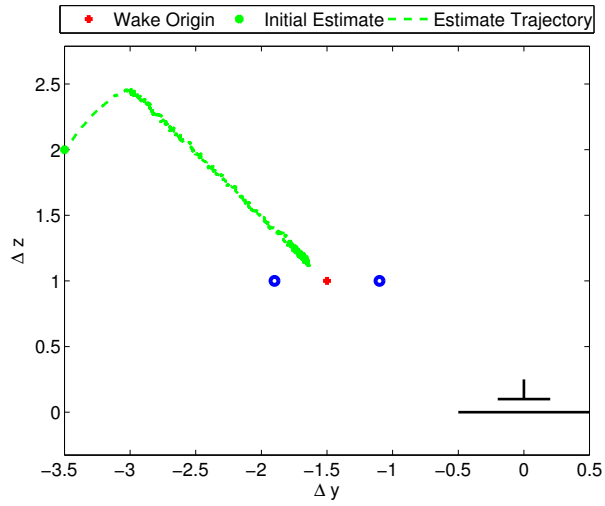


(b) Estimate Time History

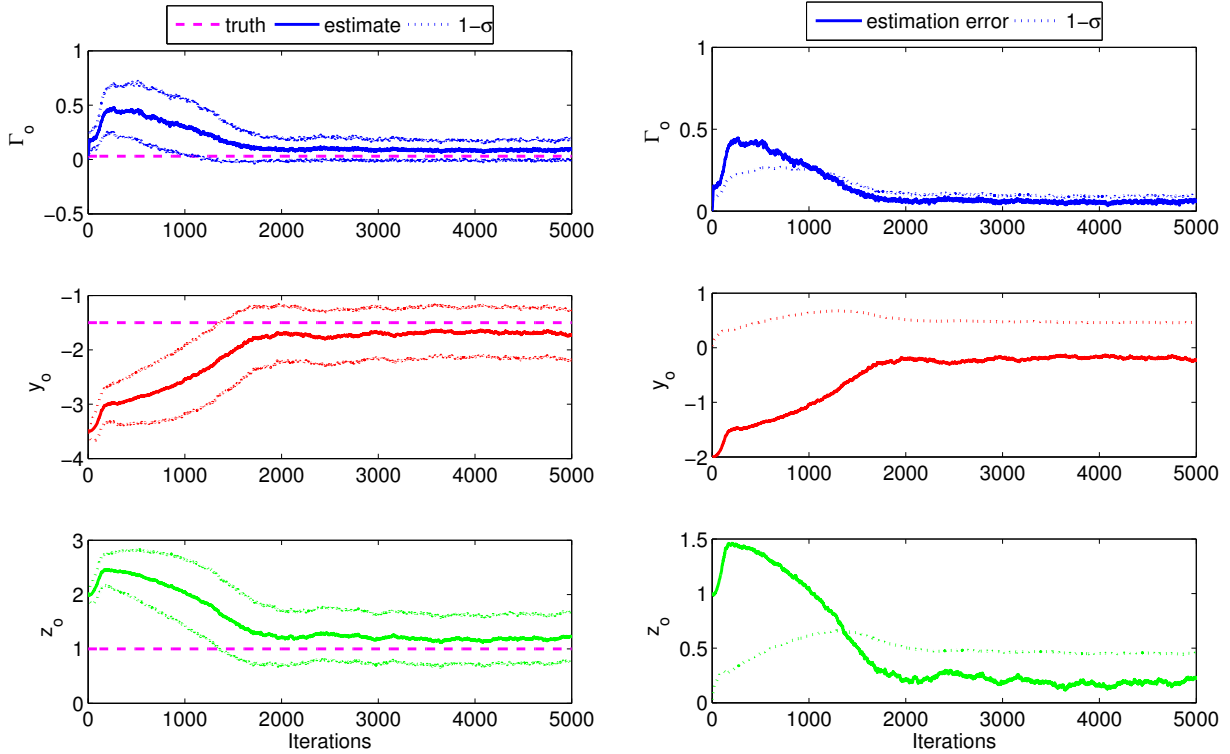


(c) Estimation Error Time History

Figure 5: Static wake simulation results for $\mathbf{x}_o = [0.03 \ -1 \ 0]^T$ (Case 1) using the EKF estimator. In the estimate trajectory map presented in (a), the vortex cores of the lead aircraft's wake are denoted by blue circles \circ and their center by a red circle \bullet , the trailing (estimating) aircraft is drawn flying into the page in black, with the initial estimate denoted by a green circle \bullet and the estimate trajectory drawn as green dashes $---$.



(a) Estimate Trajectory



(b) Estimate Time History

(c) Estimation Error Time History

Figure 6: Static wake simulation results for $\mathbf{x}_o = [0.03 \quad -1.5 \quad 1]^T$ (Case 2). The EKF estimator now takes longer to converge and has a notable bias. In the estimate trajectory map presented in (a), the vortex cores of the lead aircraft's wake are denoted by blue circles \circ and their center by a red circle \bullet , the trailing (estimating) aircraft is drawn flying into the page in black, with the initial estimate denoted by a green circle \bullet and the estimate trajectory drawn as green dashes $---$.

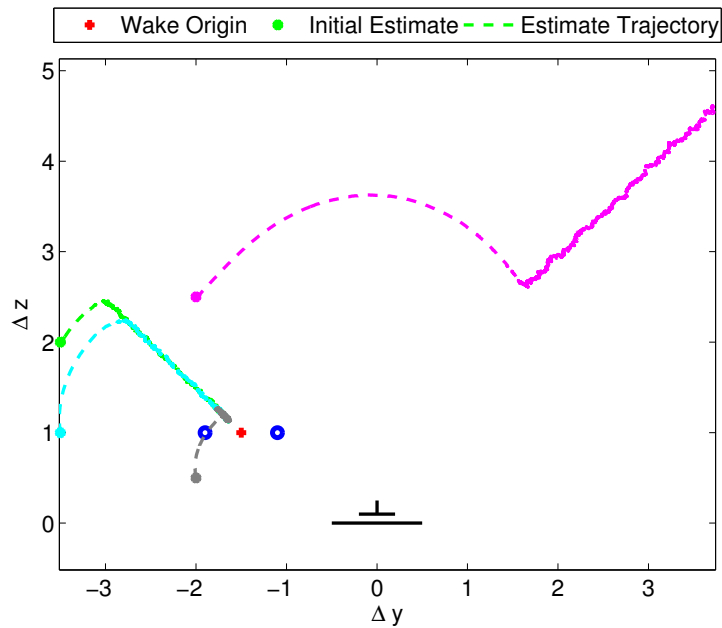
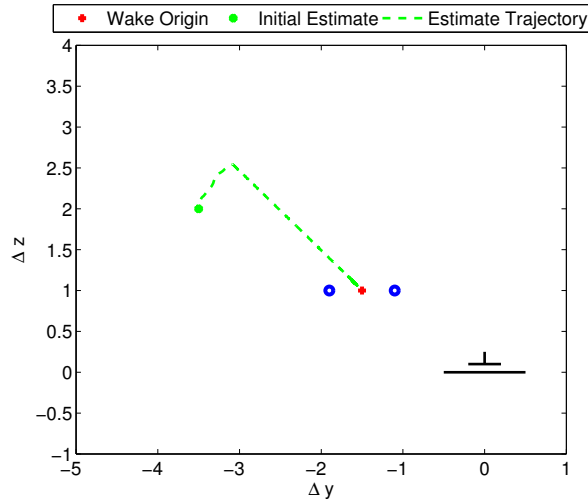
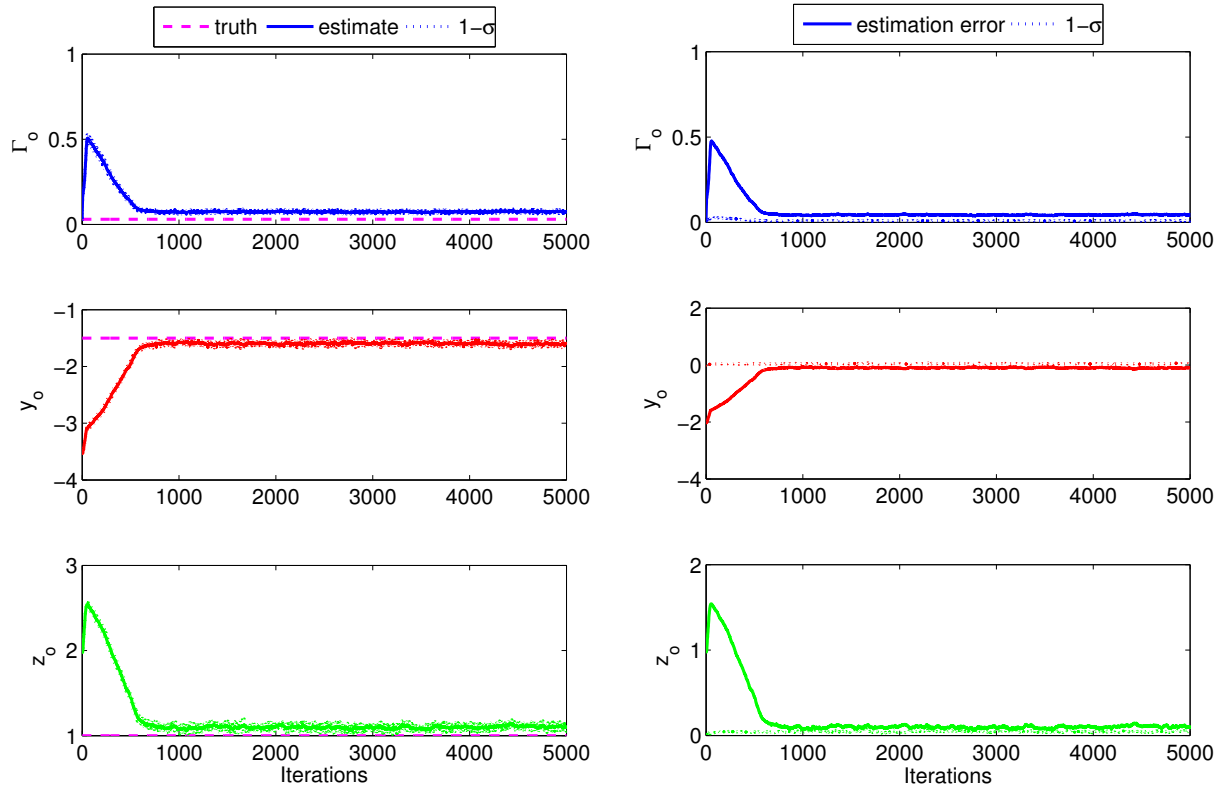


Figure 7: Estimate trajectories associated with multiple initial estimates in Case 2. The green, cyan, gray trajectories converge to the same biased estimate, while the magenta trajectory diverges. This behavior can be attributed to the wake nonlinearity and its associated observability structure. In the estimate trajectory map presented, the vortex cores of the lead aircraft's wake are denoted by blue circles \circ and their center by a red circle \bullet , the trailing (estimating) aircraft is drawn flying into the page in black, with the initial estimates denoted by circles of various colors and the corresponding estimate trajectories are drawn as dashed lines of the same color.



(a) Estimate Trajectory



(b) Estimate Time History

(c) Estimation Error Time History

Figure 8: Static wake simulation results for $\mathbf{x}_o = [0.03 \ -1.5 \ 1]^T$ (Case 2). The PF estimator results in significant decrease in the resulting biases in position and strength estimates. In the estimate trajectory map presented in (a), the vortex cores of the lead aircraft's wake are denoted by blue circles \circ and their center by a red circle \bullet , the trailing (estimating) aircraft is drawn flying into the page in black, with the initial estimate denoted by a green circle \bullet and the estimate trajectory drawn as green dashes $---$.

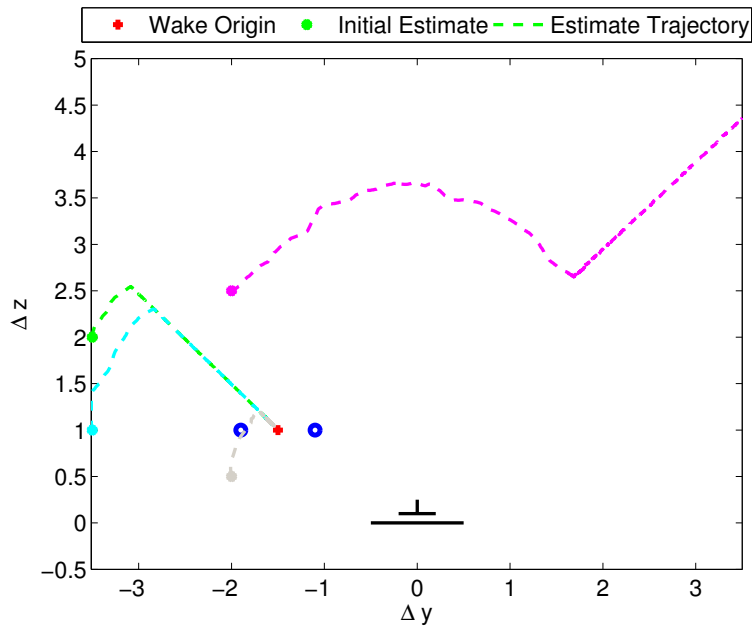
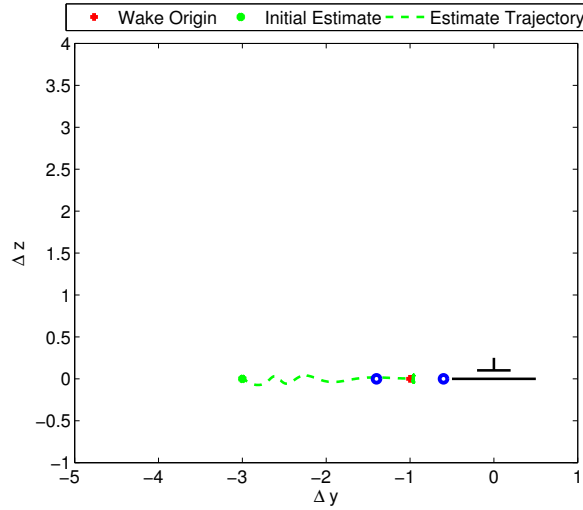
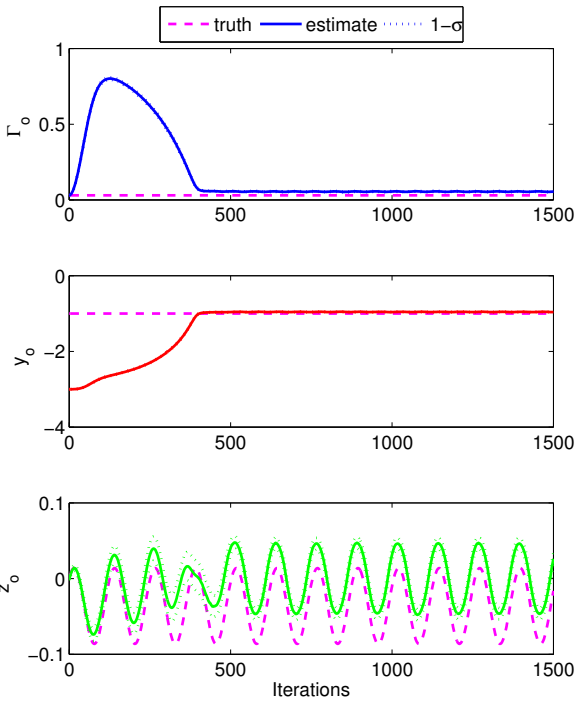


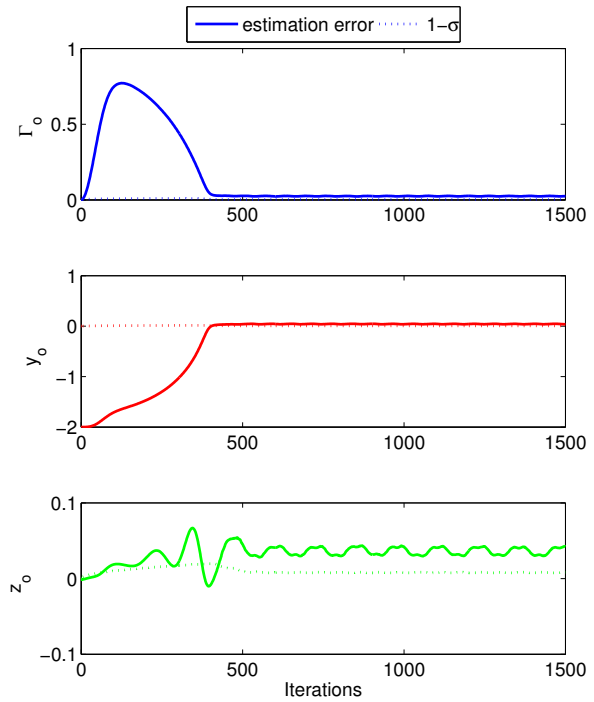
Figure 9: Estimate trajectories associated with multiple initial estimates in Case 2. The green, cyan, gray trajectories converge to the same biased estimate, while the magenta trajectory diverges. This behavior can, again, be attributed to the wake nonlinearity and its associated observability structure. In the estimate trajectory map presented, the vortex cores of the lead aircraft's wake are denoted by blue circles \circ and their center by a red circle \bullet , the trailing (estimating) aircraft is drawn flying into the page in black, with the initial estimates denoted by circles of various colors and the corresponding estimate trajectories are drawn as dashed lines of the same color.



(a) Estimate Trajectory

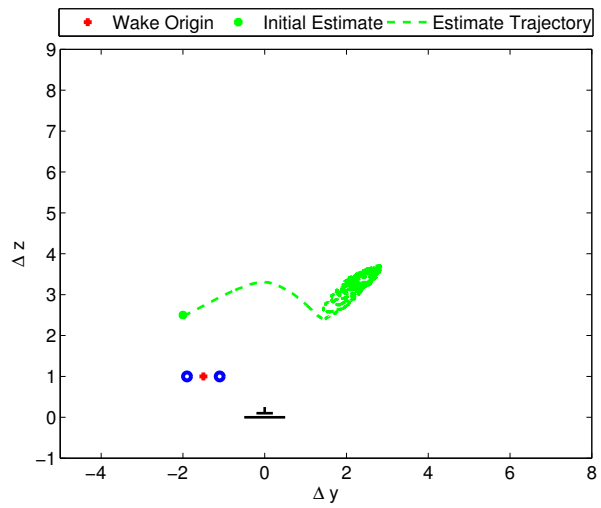


(b) Estimate Time History

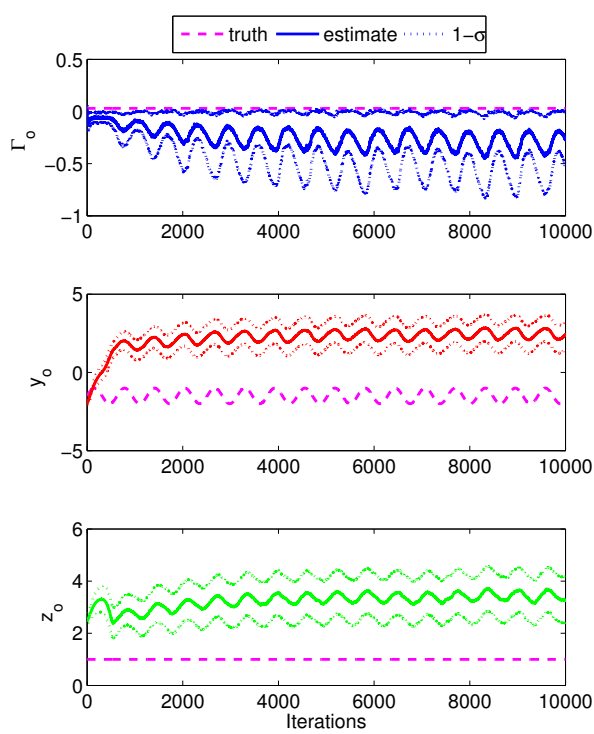


(c) Estimation Error Time History

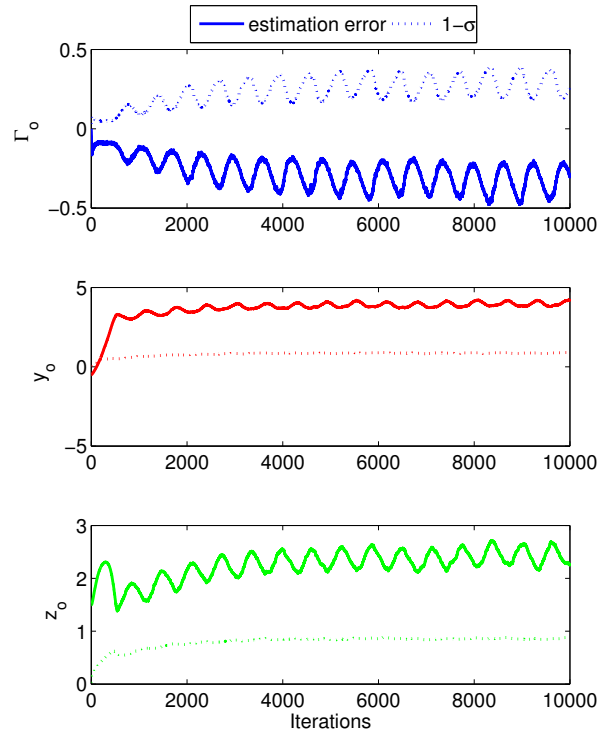
Figure 10: Relative motion simulation results for $\mathbf{x}_o = [0.03 \ -1 \ 0]^T$ with $A_1 = 0.05$, $A_2 = 0$, $\omega_1 = 0.05$ rad/s, and $\omega_2 = 0$ rad/s (Case 3). Note $\sigma_w = 1 \times 10^{-3}$ for this case only. In the estimate trajectory map presented in (a), the vortex cores of the lead aircraft's wake are denoted by blue circles \circ and their center by a red circle \bullet , the trailing (estimating) aircraft is drawn flying into the page in black, with the initial estimate denoted by a green circle \bullet and the estimate trajectory drawn as green dashes $---$.



(a) Estimate Trajectory

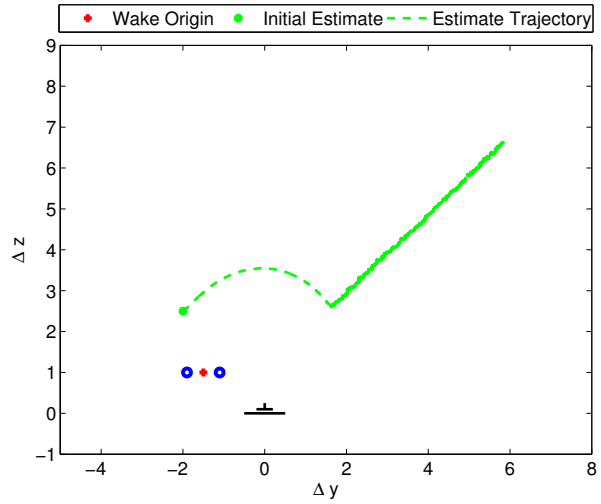


(b) Estimate Time History

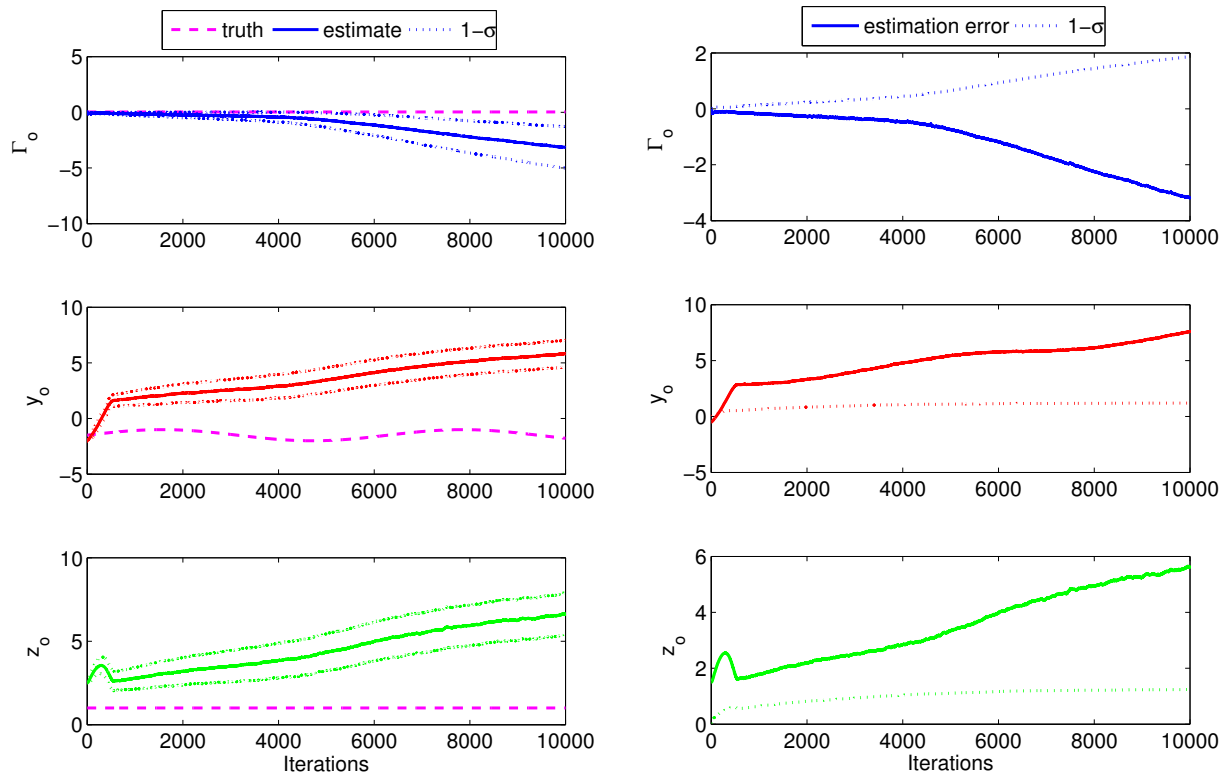


(c) Estimation Error Time History

Figure 11: Simulation identical to the static Case 2, but with relative motions prescribed as $A_1 = 0.5$, $A_2 = 0$, $\omega_1 = 0.01$ rad/s, and $\omega_2 = 0$ rad/s (Case 4a). Note the prescribed kinematics in this case are able to stabilize the estimation dynamics. In the estimate trajectory map presented in (a), the vortex cores of the lead aircraft's wake are denoted by blue circles \circ and their center by a red circle \bullet , the trailing (estimating) aircraft is drawn flying into the page in black, with the initial estimate denoted by a green circle \bullet and the estimate trajectory drawn as green dashes $---$.



(a) Estimate Trajectory



(b) Estimate Time History

(c) Estimation Error Time History

Figure 12: Relative motion simulation identical to Case 4a, but with $A_1 = 0.5$, $A_2 = 0$, $\omega_1 = 0.001$ rad/s, and $\omega_2 = 0$ rad/s (Case 4b). Note the prescribed kinematics in this case are unable to stabilize the estimation dynamics. In the estimate trajectory map presented in (a), the vortex cores of the lead aircraft's wake are denoted by blue circles \circ and their center by a red circle \bullet , the trailing (estimating) aircraft is drawn flying into the page in black, with the initial estimate denoted by a green circle \bullet and the estimate trajectory drawn as green dashes $- -$.